Polarization sensitivity contributes to multiple band spectra of one mid-infrared absorber

Yongqian Li (黎永前)*, Binbin Wang (王斌斌), Xiaolun Xu (许小轮), and Lei Su (苏 磊)

Key Laboratory of Micro/Nano Systems for Aerospace of Ministry of Education, Northwestern Polytechnical University, Xi'an 710072, China

**Corresponding author: liyq@nwpu.edu.cn*

Received May 19, 2014; accepted July 3, 2014; posted online September 26, 2014

The emerging perfect-absorber metamaterials (PAMs) provide an alternative material approach for the next generation of electromagnetic detection at any frequency band of interest. One type of dual cross-shaped PAMs is developed to obtain multiplex-band spectrum absorption at mid-infrared region. Three distinct absorption peaks are attributed to the polarization sensitivity excitation of the plasmonic resonance. The charge density distributions, which are excited by resonant electromagnetic waves passing through the PAMs medium, provide insights into the observed absorption behavior. We find that the retrieved optical properties of the PAMs including permittivity and permeability are still consistent with the sum of the Drude and Lorentz type models at wavelengths ranging from 2.0 to 10.0 μm. Such multiplex-band absorption properties enable the proposed PAMs a powerful tool for the direct detection of multiple molecular vibrational structures, and for multiple spectra infrared detection.

OCIS codes: 050.6624, 160.3918, 260.5430.
doi: 10.3788/COL201412.101603.

Plasmonic absorption metamaterials have gained tremendous interest during the past decades[1]. In the case of resonantly excited by an electromagnetic field, plasmonic absorption metamaterials have the properties of nearly perfect absorption[2,3], strong local field enhancement[4], and distinct spectral response[5]. Such optical properties promise potential applications for increasing the efficiency of photovoltaic system[6], improving the sensitivity of biological sensors[7,8], and enabling the frequency selection of photoelectric detection[9]. The plasmonic absorbers with either broad spectral features or narrow-band responses are both necessary. The broad absorption spectrum enables plasmonic absorbers blackbody-like behavior, which has promoted the techniques in fields such as sensitive photo-detection and solar harvesting[2,6]. Recently, perfect-absorber metamaterials (PAMs) with the property of multiplex-band spectral absorption attracted great attention in many fields of potential technologies[7,10]. The multiplex-band spectral response and the consequently strong enhancement of local near-field intensity have improved the intrinsic absorption cross-sections for the direct access to molecular vibrational spectra in the mid-infrared (MIR) region[8], the purpose of quantitative multiple spectroscopic bio-imaging[7,11], and the identification of pathogens fingerprinting[12].

In order to obtain the narrower multi-band absorption, variety of nanostructures with perfect absorption performance have been investigated at the wavelengths from gigahertz[13] and terahertz wave[14,15], to infrared[7,16] and even visible light[17]. Two types of structure conceiving mechanisms were employed to obtain multiplex-band resonances. One is one unit-cell structure with more than one resonant frequency[18–21]. The other strategy is kinds of hybrid structures conceived to resonate at dual or multi-frequencies. Such hybrid absorbers were first performed in terahertz[22], and then in MIR region[23,24]. To obtain multiplex-band absorption spectra, our previous work proposed a type of dual cross-shaped PAMs, which had three distinct absorption peaks at the wavelength ranging from 2.0 to 10.0 μm[25]. Here, the optical properties of the optimized configuration were investigated on the assumption of homogeneous medium. The charge distributions excited by the resonant incident electromagnetic waves were calculated to explain the multiplex-spectral absorption. The optical parameters retrieved by the scattering parameters method[26] are still consistent with the Drude and Lorentz modes, which provide a qualitative description of the multiple band spectra responses.

The proposed PAMs follow the metal–dielectric–metal scheme, as shown in Fig. 1. The dielectric layer is sandwiched by the top metallic nanoantennas layer and the ground metallic layer. The top layer consists of a periodic array of dual cross-shaped nanoantennas, which form the polarization sensitivity. The bottom layer is a continuous thick metallic film. The PAMs exhibit the properties of electromagnetic selectivity and resonance[25]. Au was used for both the top antennas and the ground conducting film. Al_2O_3 was chosen for the dielectric medium. In conjunction with the transmission blocking of the thick metallic film, the excitation of localized magnetic and electric dipole resonances produce nearly total perfect absorption at multiplex-specific frequencies[10].

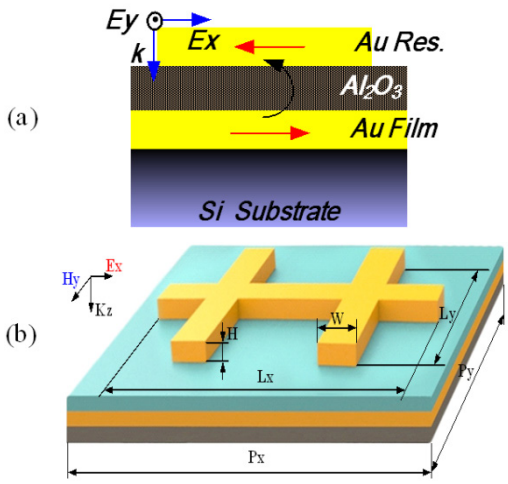

Fig. 1. Schematic representation of the PAMs: (a) metallic–dielectric–metallic layers and (b) two cross-shaped antennas connected together form the polarization sensitivity absorption.

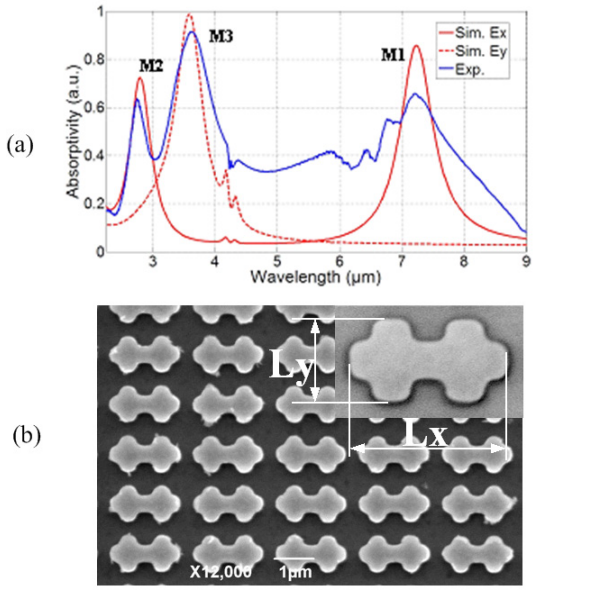

Fig. 2. (a) Normalized absorption spectra obtained from experiments and the simulations and (b) top view SEM image of the fabricated PAM sample.

The optimization of the configuration and the dimensional size was performed for the maximum absorption. To achieve the optimized effect at multiplex wavelengths, we adopted one criteria equation as[16]

$$F = \sum_{\lambda_i} \left[\left(1 - A_{\mathrm{TE}}\right) + \left(1 - A_{\mathrm{TM}}\right) \right], \tag{1}$$

where λ_i is the target wavelength and A_{TM} and A_{TE} are the absorptivities in the conditions of *Ex* and *Ey* polarized incident wave, respectively. The geometrical sizes, including the thickness of the dielectric layer and the arm lengths (*Lx*, *Ly*) were scanned to obtain the maximum electromagnetic absorption.

The electromagnetic response and the polarization properties of the proposed PAMs were investigated using commercially available finite-difference time-domain software (Lumerical Company). The permittivity of Au was modeled using a Drude expression with the plasmonic frequency of $1.32 \times 10^{16}\,\mathrm{rad}^{-1}$ and the collision frequency of $1.2 \times 10^{14}\,\mathrm{rad}^{-1}$[27]. The absorption spectra of the PAMs exhibit three distinct resonance peaks as shown in Fig. 2(a). The resonant modes of *M*1 and *M*2 are excited by the *Ex* polarized incident light, and the *M*3 mode by the *Ey* incident light. The metal–dielectric–metal layers were deposited on a Si substrate in sequence, and the pattern of the nanoantenna array was fabricated by the electron beam lithography and then followed by a lift-off process[28]. A scanning electron microscope (SEM) image of the fabricated PAMs array is shown in Fig. 2(b). The absorption spectra of the PAMs samples were characterized by a Fourier transform infrared spectrometer equipped with an infrared microscope with a normal incidence light. Although a slight difference between the theoretically calculation and experimentally measured data occurs due to the nanofabrication imperfections, the strong agreement between the experimental and the simulated absorption spectra proved that the PAM absorber has three distinct resonant wavelengths.

In contrast to polarization dependence on the absorption spectrum in Fig. 2, the thickness dependence of the dielectric layer on the resonant wavelengths was also investigated as shown in Fig. 3. The thickness of the dielectric layer plays a crucial role in determining the multiplex-band absorption. When the thickness of the dielectric layer is set to be from 20 to 65 nm, dual-band absorption of *M*2 and *M*3 can be obtained with absorptivity over 70%. Resonance modes of *M*1 and *M*2 can be achieved from 45 to 112 nm. In a narrow range of dielectric layer from 45 to 65 nm, the absorptivity bands at the triple resonance modes are greater than 70%. In the sample shown in Fig. 2, we set the thickness of dielectric layer to be 50 nm. In the condition of $Lx = 2 \times Ly$ longer than 0.8 μm, the red-shift trends of the three resonant wavelengths with the increasing arm lengths are obvious as shown in Fig. 3(b).

To better understand the multiple band responses of the proposed PAMs, the charge density distribution inside the metallic layer, which was induced by the peak wavelengths, were calculated. As shown in Fig. 4, the formation of triple resonance responses is supported by different mechanisms. Excited by the peak wavelength at mode *M*1, the induced charge distribution inside the metallic antennas forms a pattern with positive charges accumulated at one end and negative charges at another end. The same pattern but opposite arrangement occurs in the ground metal film. This characteristic is referred to the fundamental plasmonic resonance. Excited at the mode *M*3, the accumulated charges show

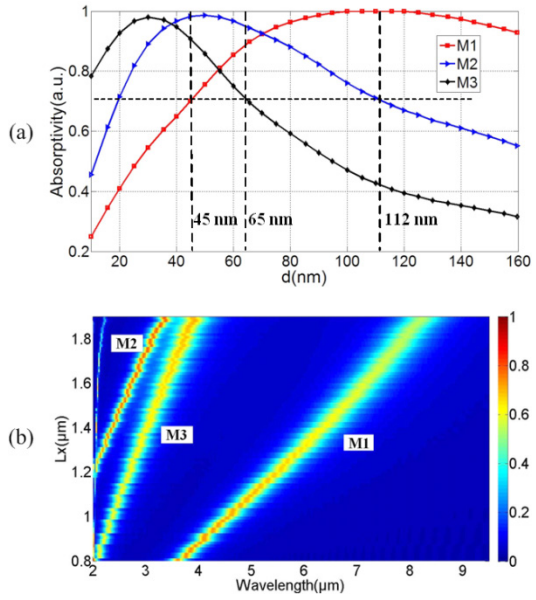

Fig. 3. (a) Dielectric layer thickness plays a crucial role in the multiple band absorption ($Lx = 1.52$ μm, $Ly = 0.92$ μm) and (b) absorption spectra are the functions of the arm lengths ($Lx = 2 \times Ly$).

one " $-$ $+$ $-$ $+$" pattern within the top antenna and one "$+$ $-$ $+$ $-$" pattern within the bottom metal film. The charge pattern divides the electric field inside the PAMs into three parts. Following the naming custom in Ref. [29], this response is termed the third-order plasmonic resonance. When the charge accumulation is excited at mode $M2$, the condition is absolutely different. The charge distribution shows the characteristic of the fundamental plasmonic resonance excited by the polarized incident light Ey. At each resonant condition, the

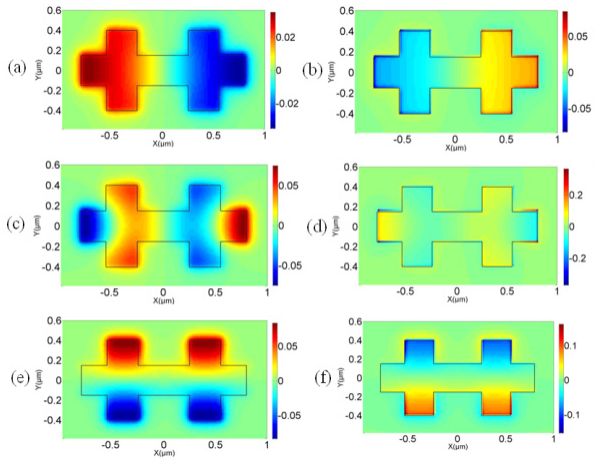

Fig. 4. Distribution of the induced charge density inside (a, c, and e) the top metal layer and (b, d and f) the bottom metal layer. The inductive charge distribute in the conditions of incident Ex polarized configuration at resonance wavelength $M1$ (a and b), $M3$ (c and d), and in the conditions of Ey incidence $M2$ (e and f). The color map represents the charge density (C/m^3), in which the blue and red colors stand for the positive and negative charges, respectively.

induced charges oscillate out of phase between the upper antennas and the lower metal layers, which produce antiparallel currents within the PAMs. In both Ey and Ex incident configurations, the antiparallel currents induce magnetic field within the dielectric layer to counteract the incident magnetic field, which corresponds to the magnetic resonance, and then results in the maximum absorption.

Optical properties of the materials present the theoretical background and interpretation between the medium and the electromagnetic field passing through them. The medium theory in terms of the effective permittivity and the effective permeability has described the macroscopic effective parameters of the metamaterials and nanostructures array[10,30]. The effective optical properties of the proposed PAMs were extracted from the transmission and reflection spectra using the robust scattering parameter retrieval method[26]. Figure 5 shows the retrieved permittivity and permeability in the conditions of Ex and Ey polarization incident electromagnetic fields. Let us examine these retrieved parameters. When electromagnetic waves propagate through a magneto-dielectric medium, the dielectric properties of the medium can be expressed as a sum of the Drude and the Lorentz terms[31]:

$$\varepsilon_{\mathrm{r}}(\omega) = \varepsilon_{\infty} - \frac{\omega_{\mathrm{p}e1}^2}{\omega^2 + \mathrm{i}\gamma_e\omega} + \sum_{j=1}^{N} \frac{\omega_{\mathrm{p}e2j}^2}{\omega_{\mathrm{o}ej}^2 - \omega^2 - \mathrm{i}\gamma_{e2j}\omega}, \quad (2)$$

$$\mu_{\mathrm{r}}(\omega) = \mu_{\infty} + \sum_{K=1}^{M} \frac{\omega_{\mathrm{p}mk}^2}{\omega_{\mathrm{o}mk}^2 - \omega^2 - \mathrm{i}\gamma_{mk}\omega}, \quad (3)$$

where μ_∞ and ε_∞ are the static permittivity and permeability at infinite frequency, respectively; ω_{o} is the resonance frequency of the electric and magnetic dipole oscillators; γ is the damping frequency; ω_{p} is the plasma frequency; the subscripts e and m represents electric and magnetic response, respectively. Above complex dielectric functions describe the intraband effects of the free-electron oscillation, and the interband effects of the bound-electron oscillation[31]. From the data curves in Figs. 5(a) and (b), we fitted the high-order Drude–Lorentz model to describe the dispersion relations of our PAMs as

$$\varepsilon_{\mathrm{r}}(\omega) = 1 - \frac{3651.1^2}{\omega^2 + 0.4\cdot\mathrm{i}\omega} + \frac{1132.0^2}{718.1^2 - \omega^2 - 15.2\cdot\mathrm{i}\omega} + \frac{2008.3^2}{291.1^2 - \omega^2 - 23.2\cdot\mathrm{i}\omega}, \quad (4)$$

$$\mu_{\mathrm{r}}(\omega) = 3.0 + \frac{358.3^2}{685.4^2 - \omega^2 - 21.8\cdot\mathrm{i}\omega} + \frac{213.7^2}{261.8^2 - \omega^2 - 22.1\cdot\mathrm{i}\omega}, \quad (5)$$

where the unit of frequency is terahertz ($\times$ 10^{12} Hz). The assumption of $\varepsilon_m = 1.0$ and $\mu_m = 3.0$ implies the contribution of bound electrons. The quasi-static

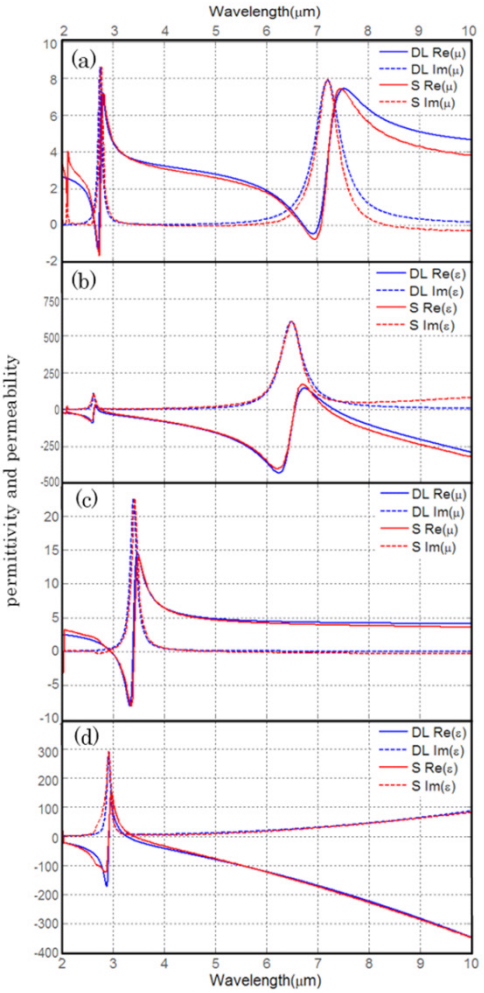

Fig. 5. Optical properties of the PAMs retrieved by scattering parameters method and described by the sum of the Drude–Lorentz modes in the condition of (a, b) *Ex* and (c, d) *Ey* polarized incident configurations.

Drude–Lorentz formula in Eq. (4) describes the dual-band permittivity of the PAMs. The permeability resonance follows the higher order Lorentz model. The optical curves in Figs. 5(c) and (d) are described as

$$\varepsilon_{\mathrm{r}}(\omega) = 1 - \frac{3658.9^2}{\omega^2 + 45.8 \cdot \mathrm{i}\omega} + \frac{1834.4^2}{644.4^2 - \omega^2 - 18.2 \cdot \mathrm{i}\omega}, \quad (6)$$

$$\mu_{\mathrm{r}}(\omega) = 3.0 + \frac{548.8^2}{554.4^2 - \omega^2 - 24.0 \cdot \mathrm{i}\omega}. \quad (7)$$

The electric responses of the permittivity satisfy the combination of the Drude and Lorentz model, although the permeability resonance follows the Lorentz type. The optical properties of our PAMs are consistent with the sum of the Drude and Lorentz model in the MIR region from 2.0 to 10.0 μm. In view of the prerequisite for homogenization[30], the microscopic spatial fields distributions and the polarization currents inside the PAMs vary sharply between adjacent unit cells, and the waves propagating through the medium are not smoothened.

In conclusion, we demonstrate a type of dual cross-shape PAM for the purpose of achieving multiple band absorption spectra in MIR region. Stimulated by the *Ex* and *Ey* polarized incident electromagnetic wave, the optimized PAMs display three distinct absorption peaks. In contrast to the earlier implementations of the polarization-independent prefect absorber, the polarization sensitivity of the proposed PAMs contributes to the achievement of multiplex-band absorption spectra, which is revealed by the induced charge density distribution within the PAMs. The retrieved optical properties of the PAMs describe the fundamental resonance modes and higher order modes, which are still consistent with the sum of the Drude and Lorentz model in the MIR region of wavelengths ranging from 2.0 to 10.0 μm. The determination of the key parameters in the Drude and Lorentz modes still needs further investigation in future work. The pronounced sharp and independent absorption spectra features enable the PAMs attractive applications in the label-free identification scheme to detect the structural binding characteristics of bio-molecular, and to identify the separated multiple molecular vibrational stretches[12].

This work was supported by the National Natural Science Foundation of China (No. 51175436), the Aeronautical Science Foundation of China (No. 2012ZC53036), the Northwestern Polytechnical University Foundation for Fundamental Research (No. NPU-FFR-JC200811), and the 111 Projects from Chinese Ministry of Education (No. B13044).

References

1. C. M. Watts and X. Liu, Adv. Mater. **24,** OP98 (2012).
2. V. G. Kravets, F. Schedin, and A. N. Grigorenko, Phys. Rev. B **78,** 205405 (2008).
3. N. I. Landy, S. Sajuyigbe, J. J. Mock, and D. R. Smith, Phys. Rev. Lett. **100,** 20740 2(2008).
4. B. Liu and S. Shen, Phys. Rev. B **87,** 115403 (2013).
5. X. Liu, T. Starr, A. F. Starr, and W. J. Padilla, Phys. Rev. Lett. **104,** 207403 (2010).
6. C. Hägglund and S. P. Apell, Phys. Chem. Lett. **3,** 1275 (2012).
7. K. Chen, R. Adato, and H. Altug, ACS Nano **6,** 7998 (2012).
8. Y. Li, L. Su, C. Shou, C. Yu, J. Deng, and Y. Fang, Sci. Rep. **3,** 2865 (2013).
9. S. Ogawa, K. Okada, N. Fukushima, and M. Kimata, Appl. Phys. Lett. **100,** 021111 (2012).
10. J. Hao, L. Zhou, and M. Qiu, Phys. Rev. B **83,** 165107 (2011).
11. Y. C. Lai, H. C. Lee, S. W. Kuo, C. K. Chen, H. T. Wu, O. K. Lee, and T. J. Yen, Adv. Mater. **24,** 148 (2012).
12. R. Adato, A. A. Yanik, J. J. Amsden, D. L. Kaplan, F. G. Omenetto, M. K. Hong, S. Erramilli, and H. Altug, Proc. Natl Acad. Sci. USA **106,** 19227 (2009).
13. J. Yu, H. Chen, X. Yu, and S. Liu, Chin. Opt. Lett. **12,** S11301 (2014).

14. D. Zhang, Q. Wen, and Y. Xie. Chin. Opt. Lett. **9,** S10402 (2011).
15. M. Pu, M. Wang, C. Hu, C. Huang, Z. Zhao, Y. Wang, and X. Luo, Opt. Express **20,** 25513 (2012).
16. Z. H. Jiang, S. Yun, D. H. Werner, and T. S. Mayer, ACS Nano **5,** 4641 (2011).
17. J. Hao, J. Wang, X. Liu, W. J. Padilla, L. Zhou, and M. Qiu, App. Phys. Lett. **96,** 251104 (2010).
18. B. Zhang, Y. Zhao, Q. Hao, B. Kiraly, I. Khoo, S. Chen, and T. J. Huang, Opt. Express **19,** 15221 (2011).
19. N. Zhang, P. Zhou, D. Cheng, X. Weng, J. Xie, and L. Deng, Opt. Lett. **38,** 1125 (2013).
20. C. Wu, I. B. Neuner, G. Shvets, J. John, A. Milder, B. Zollars, and S. Savoy, Phys. Rev. B **84,** 075102 (2011).
21. J. Wang, C. Fan, P. Ding, J. He, Y. Cheng, W. Hu, G. Cai, E. Liang, and Q. Xue, Opt. Express **20,** 14871 (2012).
22. J. Grant, Y. Ma, S. Saha, L. B. Lok, A. Khalid, and D. Cumming, Opt. Lett. **36,** 1524 (2011).
23. J. Hendrickson, J. Guo, B. Zhang, W. Buchwald, and R. Soref, Opt. Lett. **37,** 371 (2012).
24. W. Ma, Y. Wen, and X. Yu, Opt. Express **21,** 30724 (2013).
25. Y. Qian and E. A. Li, Proc. SPIE **9099,** 37 (2014).
26. D. R. Smith, D. C. Vier, T. Koschny, and C. M. Soukoulis, Phys. Rev. E **71,** 036617 (2005).
27. P. B. Johnson and R. W. Christy, Phys. Rev. B**6,** 4370 (1972).
28. A. Boltasseva and V. M. Shalaev, Metamaterials **2,** 1 (2008).
29. D. Denkova, N. Verellen, A. V. Silhanek, V. K. Valev, P. V. Dorpe, and V. V. Moshchalkov, ACS Nano **7,** 3168 (2013).
30. C. R. Simovski, J. Opt. **13,** 013001 (2011).
31. A. D. Rakic, A. B. Djurišic, J. M. Elazar, and M. L. Majewski, App. Opt. **37,** 5271 (1998).